AFIT/GEO/ENG/92D-06

The Effect of an Adaptive Optical System's Spatio-Temporal Response on Imaging Performance

THESIS

Patrick Michael Harrington
Captain, USAF

AFIT/GEO/ENG/92D-06

AFIT/GEO/ENG/92D-06

The Effect of an Adaptive Optical System's Spatio-Temporal Response on Imaging Performance

THESIS

Presented to the Faculty of the School of Engineering

of the Air Force Institute of Technology

Air University

In Partial Fulfillment of the

Requirements for the Degree of

Master of Science in Electrical Engineering

Patrick Michael Harrington, B.S.E.

Captain, USAF

December, 1992

Table of Contents

List of Figures

Abstract

Ideally, an adaptive optical control system would have instantaneous temporal response and infinite spatial bandwidth. In real systems, the response time of the adaptive optical control system is limited by the integration time of the wave front sensor, the computational time of the control algorithm, and the actuator response time. Additionally, finite inter actuator spacing limits the deformable mirror's ability to reproduce spatial frequencies having a period less than twice this spacing. Although analyses general enough to account for both the temporal and spatial characteristics of the adaptive optical system exist, they are complex and require detailed information regarding the wave front sensor, the deformable mirror, and the control algorithm. This investigation develops a frequency domain model that describes performance effects of an adaptive optical system's temporal response taking into account aperture piston and tilt removal and spatial bandwidth limitations due to finite subaperture size. The unique aspect of this model is the relative ease with which performance characteristics of different spatial and temporal system response functions can be investigated.

The Effect of an Adaptive Optical System's Spatio-Temporal Response on Imaging Performance

I. Introduction.

1.1 Background.

Adaptive optics are used to improve the real time imaging capabilities of large ground based telescopes (9). As light from a celestial source passes through the earth's atmosphere, it suffers random phase delays across its wave front. These phase delays are caused by turbulence induced fluctuations in the atmosphere's index of refraction. Because of the effect of atmospheric turbulence, very large diameter telescopes have little more resolving power than telescopes 0.1 to 0.2 meters in diameter (15)(19). By measuring and compensating for wave front distortions, adaptive optics make it possible to achieve near diffraction limited performance of these same very large telescopes (4). Figure 1.1 depicts a typical adaptive optic system. First, turbulence induced phase distortions of a reference wave front are measured by a wave front sensor. This phase information is then used by a computer to determine the optimal actuator weightings across the deformable mirror. Typically, the computer implements an algorithm that minimizes the mean square error between the unaberrated reference wave front and the wave front predicted to arrive at the image sensor. Lastly, the phase distortions are corrected at the deformable mirror surface by complementary path length adjustments across the wave front, and the object of interest is imaged.

Ideally, an adaptive optical control system would have instantaneous temporal response and infinite spatial bandwidth. In real systems, the response time of the adaptive optical control system is limited by the integration time of the wave front sensor, the computational time of the control algorithm, and the actuator response time. Additionally, finite inter actuator spacing limits the deformable mirror's ability to reproduce spatial frequencies having a period less than twice this spacing (19). As any one of these system parameters can be the limiting

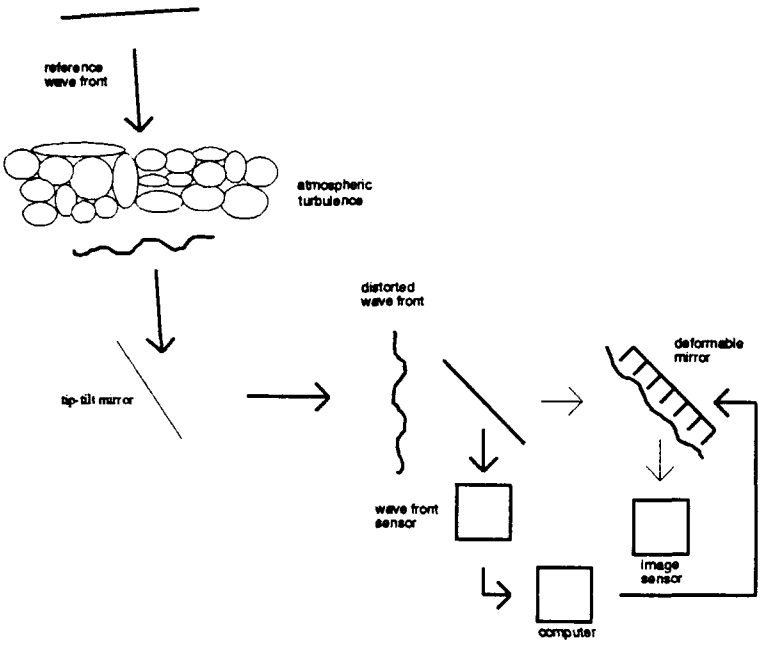

Figure 1.1. Representation of an adaptive optical system correcting for atmospheric tubulence.

factor in the system's imaging performance, it is invaluable in system design to have simple equations or models that provide a point of departure for each parameter.

Response time, from wave front detection through actuator positioning, limits system performance because the phase distortions across the wave front are continually changing in time. This results in an incorrect matching between the deformable mirror and the aberrated wave front, especially for higher frequencies. In two recent papers, Fried and Karr independently investigated the effect of time delay on the servo control loop of an adaptive optical system (11)(2). Although their approaches are slightly different, both made the same assumptions and determined the mean square phase error between the actual wave front and the sensed wave front to be:

$$\sigma^2 = 28.4\,(f_G \Delta t)^{\frac{5}{3}} \tag{1.1}$$

where f_G is the well known Greenwood frequency and Δt is time delay between wave front sensing and actuator repositioning (6). In their derivations Fried and Karr neglected the spatial frequency limitations of the deformable

mirror and approximated the atmospheric turbulence power spectrum by its high frequency asymptote ignoring the inherent removal of piston and the possibility of tilt correction over the aperature. They also neglected temporal bandwidth limitations due to the finite integration time of the wave front sensor, causing an unrealistic equal weighting of all temporal frequencies across the spectrum. By equally weighting all frequencies, Fried and Karr's results also reflect a higher than expected value of the mean square error for any time delay Δt. As the delay time becomes longer, lower spatial frequency corrections of the deformable mirror become uncorrelated with the incoming wave front increasing the residual mean square error.

The above cited analyses have broad applicability to systems that have both a wide spatial bandwidth and very fast response time. Adaptive optical systems that meet these requirements are normally built only for smaller aperture telescopes. The complexity and expense involved in producing adaptive optical systems that attempt to meet these requirements for larger telescopes have driven designers to considering partial spatial compensation (16). Systems that implement partial compensation have a lower spatial bandwidth and are not adequately modeled by Eq (1.1). Although analyses general enough to account for both the temporal and spatial characteristics of the adaptive optical system exist, they are complex and require detailed information regarding the wave front sensor, the deformable mirror, and the control algorithm (22)(21).

1.2 Objective

The primary objective of this investigation is to develop a frequency domain approach, using linear systems methods, that describes performance effects of an adaptive optical system's temporal response taking into account aperture piston and tilt removal and spatial bandwidth limitations due to finite subaperture size. The secondary objective is to address when use of our approach yields substantially different results than those of Fried and Karr.

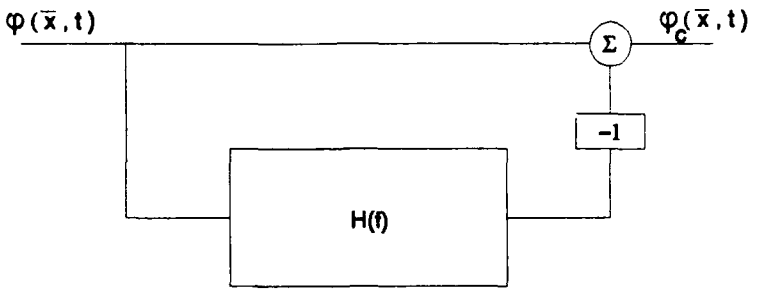

Figure 1.2. Block diagram of an adaptive optical system's transfer function.

1.3 Approach

In this investigation, a frequency domain approach is used to predict the mean square value of the residual phase error of a corrected wave front, $\varphi_c(\vec{x}, t)$. Modeling the system transfer function of the adaptive optical system as shown in Figure 1.2, the residual phase error of $\varphi_c(\vec{x}, t)$ can be shown to equal:

$$\sigma^2 = \int_{-\infty}^{\infty} \mathrm{d}f \ |1 - H(f)|^2 W(f) \tag{1.2}$$

where $W(f)$ is the temporal power spectrum of the wave front phase fluctuations due to atmospheric turbulence, $\varphi(\vec{x}, t)$, and $H(f)$ is the transer function of the adaptive optical system. The input spectrum, $W(f)$, is derived as the Fourier transform of the temporal covariance, $C_\varphi(\tau) = \langle \varphi(\vec{x}, t)\varphi(\vec{x}, t + \tau) \rangle$, and will be developed to account for inherent piston removal and tilt removal capability of present adaptive optical systems using methods developed by Greenwood and Fried (8). The filtering action of the transfer function will be assumed to be separable in time and space so that $H(f) = H_T(f) \cdot H_S(f)$, where $H_T(f)$ accounts for the system's temporal delay and bandwidth and $H_S(f)$ is the temporal equivalent spatial response of the deformable mirror. It is important to note here that all filtering, both temporal and spatial, will be done in the temporal frequency domain. For a given wave front spectrum, $W(f)$, this approach lends itself to the investigation of arbitrary filter functions due to the simple multiplication operations required to account for the filtering response in Eq (1.2). This will be shown to be especially true of the temporal transfer function $H_T(f)$.

1.4 Overview of Thesis

Chapter II reviews Greenwood and Fried's method of developing a piston and tilt removed spectrum of wave front corrections for an adaptive optical system. Chapter III developes the temporal spectrum of wave front phase aberations acounting for piston and tilt and developes a method for determining the temporal equivalent spatial response of the deformable mirror. In chapter IV the result of the preceding chapter is evaluated for values of interest to current system designers and compared to results using Karr's and Fried's models. Conclusions are drawn and recommendations made in chapter V.

II. Literature Review.

This chapter reviews Greenwood and Fried's (GF) often referenced paper which describes the power spectra of wave front corrector motion for circular correcting subapertures of a larger segmented circular mirror (8). In their analyses, the correcting subapertures of the system are capable of independent piston and tilt motion, and the power spectra for both types of motion are developed. Additionly, GF account for overall piston and the possibility of overall tilt correction prior to the wave front reaching the segmented mirror. It is this aspect of their development that is particularly useful in this investigation. Figure 2.1 depicts the wave front correction process modeled by GF. Tilt of the wave front is removed as the best fit plane through the center of an aperture. The center position of a correcting subaperture is given by $\vec{r}_1$ and is referenced from the center of the overall aperture, (see Figure 2.2). By allowing the subaperture size of the segmented mirror to approach zero, the piston and tilt removed spectrum of the incident wave front phase can be approximated by the piston and tilt removed spectrum of the subaperture's piston motion at each point on the mirror.

To begin statistical modeling of a subapertures piston motion, it is first necessary to have an expression for the vertical position of the subapertures as a function of time. GF find the time dependant piston position of a subaperture of diameter d centered at position $\vec{r}_1$ to be

$$\tilde{\varphi}(t) = \overline{\varphi(\vec{x},t)} - \overline{\overline{\varphi(\vec{x},t)}} - 16nD^{-2}\vec{r}_1 \cdot \overline{\overline{\vec{x}\varphi(\vec{x},t)}} \tag{2.1}$$

where a single overbar denotes a spatial average over the subaperture, the double overbar denotes a spatial average over the overall aperture of radius D, and $\varphi(\vec{x},t)$ the phase of the wave front prior to any corrections. The first term of Eq (2.1) represents the average phase of the wave front over a subaperture centered at $\vec{r}_1$ in the aperture at time t. Term two represents the average phase of the wave front over the entire aperture and its inclusion accounts for the system's insensitivity to aperture piston. Lastly, term three accounts for the possibility of aperture tilt removal by the adaptive optical system. In this equation, $n = 1$ indicates aperture tilt removal and $n = 0$ that no such compensation has occured.

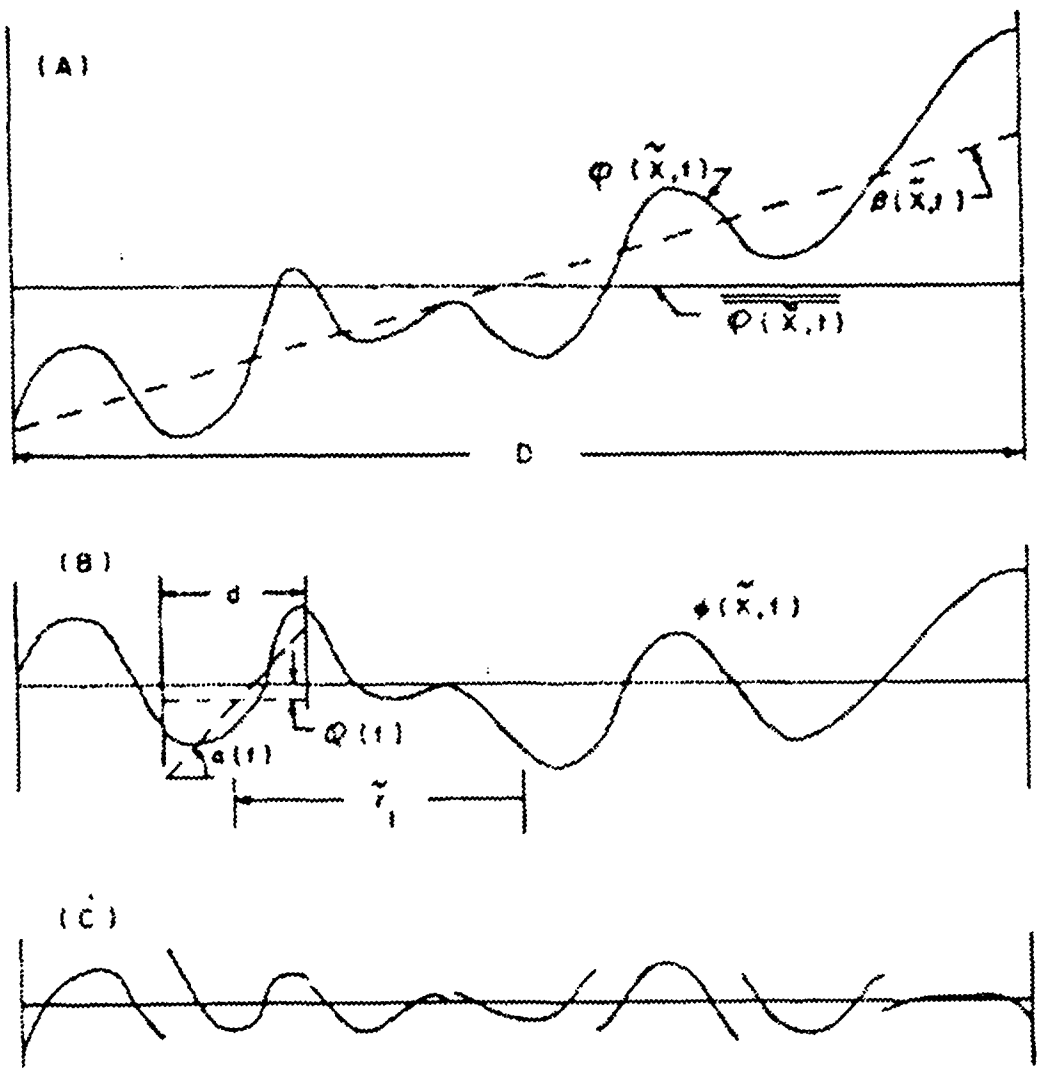

Figure 2.1. "A one-dimensional representation of wave-front correction (vertical scale greatly expanded). (A) Initial wave front at aperture plane, (B) wave front after overall tilt correction; local piston and tilt shown for segment of size $d = D/7$, (C) residual wave front after compensation over all segments. (8)."

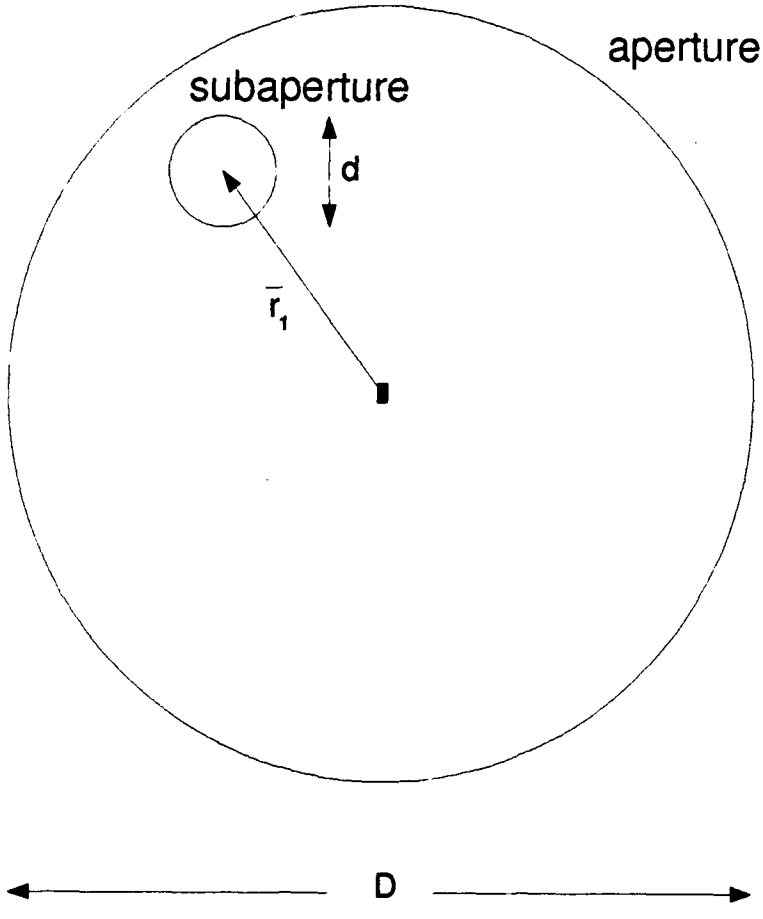

Figure 2.2. Top view of a subaperture centered at position $\vec{r}_1$.

To determine the power spectral density or spectrum of a real, stationary, zero mean, random process, we first need to determine its covariance function. Fourier transforming the covariance function results in the power spectral density. The temporal covariance of $\varphi(t)$ is defined as

$$C_{\tilde{\varphi}}(\tau) = \langle \tilde{\varphi}(t)\, \tilde{\varphi}(t+\tau) \rangle. \tag{2.2}$$

GF substitute Eq (2.1) in Eq (2.2) and find the temporal covariance can be written in the following form:

$$C_{\tilde{\varphi}}(\tau) = \int \mathrm{d}\vec{r}\; C_{\delta\varphi}(\vec{r},\tau)\, T_{\varphi}(\vec{r}) \tag{2.3}$$

where $C_{\delta\varphi}(\vec{r},\tau) = \langle \varphi(\vec{x},t)\, \varphi(\vec{x}+\vec{r},t+\tau) \rangle$ and $T_{\varphi}(\vec{r})$ is a transfer function defining the effects of piston and tilt removal at single points in the aperture. GF find $T_{\varphi}(\vec{r})$ to have the following form for a subaperture size that approaches zero:

$$T_{\varphi}(\vec{r}) = \delta(r) + S_1(\vec{r}) - S_2(\vec{r}) \tag{2.4}$$

where

$$S_1(\vec{r}) = \frac{8}{(\pi D)^2} \begin{cases} \left\{4n\left(\frac{r_1}{D}\right)\left[\left(\frac{r_1}{D}\right) + \left(\frac{r}{D}\right)\cos(\theta-\phi)\right] + 1\right\} \\ \times \left\{\arccos\left(\frac{r}{D}\right) - \left(\frac{r}{D}\right)\left[1 - \left(\frac{r}{D}\right)^2\right]^{\frac{1}{2}}\right\} \\ -\frac{8}{3}n\left(\frac{r}{D}\right)\left(\frac{r_1}{D}\right)^2\left[1-\left(\frac{r_1}{D}\right)^2\right]^{\frac{3}{2}}\left[1+4\cos^2(\theta-\phi)\right], & 0 \le \left(\frac{r}{D}\right) \le 1 \\ 0, & 1 \le \left(\frac{r}{D}\right) \end{cases} \tag{2.5}$$

and

$$S_2(\vec{r}) = \frac{8}{\pi D^2} \begin{cases} 1 + 4n\left(\frac{r_1}{D}\right)\left[\left(\frac{r_1}{D}\right) + \left(\frac{r}{D}\right)\cos(\theta-\phi\right], & 0 \le \left(\frac{r_2}{D}\right) \le \frac{1}{2} \\ 0, & \frac{1}{2} \le \left(\frac{r_2}{D}\right) \end{cases} \tag{2.6}$$

and $r = \frac{|\vec{r}|}{D}$, r_1 is the vector specifying the point of interest in the aperture, $\theta = \arg(\vec{r})$, $\phi = \arg(\vec{r}_1)$, and $r_2 = \sqrt{r^2 + r_1^2 + 2rr_1\cos(\theta-\phi)}$. The actual derivation of the transfer function, $T_{\varphi}(\vec{r})$, is presented by GF. It is important to recognize at this point that $C_{\varphi}(\tau)$ represents the covariance over a subaperture with zero diameter

located at $\vec{r}_1$ and not over the entire aperture. Recall, we are considering a subaperture size that approaches zero diameter to approximate the incident wave front phase.

GF use the following relationship to determine $C_{\delta\varphi}(\vec{r},\tau)$:

$$C_{\delta\varphi}(\vec{r},\tau) = C_{\delta\varphi}(0,\tau) - \frac{1}{2} D_{\delta\varphi}(\vec{r},\tau) \tag{2.7}$$

where $D_{\delta\varphi}(\vec{r},\tau)$ is the called the phase structure function by GF and is defined as:

$$D_{\delta\varphi}(\vec{r},\tau) = \langle [\varphi(\vec{x},t) - \varphi(\vec{x}+\vec{r},t)][\varphi(\vec{x},t+\tau) - \varphi(\vec{x}+\vec{r},t+\tau)] \rangle \tag{2.8}$$

Substituting Eq (2.7) in Eq (2.3), GF arrive at the important result:

$$C_{\dot{\varphi}}(\tau) = -\frac{1}{2} \int d\vec{r}\; D_{\delta\varphi}(\vec{r},\tau)\, T_{\varphi}(\vec{r}) \tag{2.9}$$

where as shown by GF:

$$\int d\vec{r}\; T_{\varphi}(\vec{r}) = 0. \tag{2.10}$$

Note the inclusion of the delta function term in Eq (2.4). GF validate Eq (2.10) for a nonzero subaperture diameter, d, and when discussing the single point phase spectrum, state the delta function term can be disregarded. This is only half true. The delta function has no impact on Eq (2.9) but is in fact necessary for Eq (2.10) to be valid.

Eq (2.9) can be Fourier transformed to give the single point temporal power spectrum of piston motion:

$$W_{\dot{\varphi}}(f) = -\frac{1}{2} \int d\vec{r}\; W_{\delta\varphi}(\vec{r},f)\, T_{\varphi}(\vec{r}) \tag{2.11}$$

where $W_{\delta\varphi}(\vec{r},f)$ is the temporal Fourier transform of the phase difference structure function introduced in Eq (2.8). This spectra will subsequently be referred to as the phase-difference spectrum.

To evaluate Eq (2.11), only $W_{\delta\varphi}(\vec{r}, f)$ requires definition. GF mistakenly reference Lee and Harp (12) (they should have referenced Tatarski (18)) and define the single layer phase-difference power spectrum for a plane wave reference as:

$$W_{\delta\varphi}(\vec{r}, f) = 2.079(f/f_n)^{-8/3}(f_n)^{-1} \times (D/r_o)^{5/3}\sin^2(fr/f_n) \tag{2.12}$$

where $f_n = \frac{v}{D\pi}$ is a normalizing variable that accounts for wind velocity, v, and aperture diameter, D, r_o is Fried's coherence length (a measure of the strength of a layer of atmospheric turbulence) (3), and $r = |\vec{r}|$. GF arrive at Eq (2.12) by simplifying the vectoral nature of $W_{\delta\varphi}(\vec{r}, f)$. GF assume the vector $\vec{r}$ and the wind velocity $\vec{v}$ are parallel for every pair of points across the aperture. The significance of this assumption will be clarified in the next chapter. This definition of the phase difference power spectrum also assumes a Kolmogorov spectrum of the atmospheric refractive index fluctuations with an infinite outer scale and an infinitely small inner scale.

GF evaluate Eq (2.11) for the above phase difference spectrum and present their result in graphical form. For perfect spatial wave front reconstruction, $d = 0$, they find the high frequencies roll off as $f^{-8/3}$ and are unaffected by piston and tilt correction. Regardless of subaperture size, GF find the low frequencies roll off as either $f^{-4/3}$ for overall tilt removal or $f^{-2/3}$ for no tilt removal. GF also provide the necessary transfer functions to evaluate Eq (2.11) for the case of non-zero subaperture size. The resulting spectra would include the effects of piston and tilt removal and also finite bandwidth limitations of the deformable mirror. Initially, it seems it may be possible to use the asymtotic approximations to represent the temporal phase spectrum of an incoming aberrated wave front corrected for overall piston and tilt. However, the GF spectrum plots and approximations are not valid models for the low frequency behavior of a piston and tilt phase spectrum. This is attributable to the non-realizable assumption that the phase difference power spectrum is non-vectoral in nature (7). Eq (2.11) and the transfer function $T_{\varphi}(\vec{r})$ are valid however, and in Chapter III, these equations will be used to determine a more realistic single point phase power spectrum that accounts for aperture piston and tilt removal.

III. Methodology

As stated briefly in Chapter I, Eq (1.2) will be used to model the mean square phase error performance of an adaptive optical system. Before this equation can be used however, an expression must be developed for each of the individual terms with respect to the temporal frequency variable f. Section 3.1 will introduce the spectrum of the refractive index fluctuations in the atmosphere and develop the associated temporal spectrum, $W_\varphi(f)$, of the phase fluctuations $\varphi(\vec{x},t)$. Section 3.2 will develop the aperture piston and tilt removed temporal spectrum, $W_{\tilde{\varphi}}(f)$, of these same phase fluctuations. Lastly, section 3.3 will develop the method by which spatial bandwidth limitations will be accounted for in the transfer function $H_S(f)$.

3.1 Phase fluctuations for the von Karmen spectrum

This section introduces the von Karman spectrum to characterize the refractive index fluctuations of turbulent eddies in the atmosphere. From this spectrum, the spatial and temporal spectra of the wave front phase is determined. The temporal phase spectrum will be that of the reference wave front just prior to aperture tilt correction.

The 3-dimensional von Karmen spectrum of refractive index fluctuation has the following form:

$$\Phi_n(k_t) = \frac{0.033C_n^2}{\left(k_t^2 + k_o^2\right)^{\frac{11}{6}}} e^{\frac{-k_t^2}{k_m^2}} \tag{3.1}$$

where k_t is the spatial wave number, $k_o = \frac{2\pi}{L_o}$, $k_m = \frac{2\pi}{l_o}$, and C_n^2 is a measure of the strengh of the atmospheric tubulence. L_o and l_o are the outer and inner scales of the atmospheric turbulence eddy size. This spectrum is a variation of the Kolmogorov spectrum, given by:

$$\Phi_n(k_t) = 0.033C_n^2 k_t^{\frac{-11}{3}}. \tag{3.2}$$

Goodman notes that the power in the spectrum below k_o has not been characterized to date, and that the von Karmen spectrum is only an artificial means of eliminating the pole at $k_t = 0$ in the Kolmogorov spectrum (5).

Given $\Phi_n(k_t)$, we can determine the 2-dimensional spatial spectrum of the phase fluctuations of a plane wave passing through a turbulent medium as

$$F(k_t) = \pi \bar{k}^2 L \left(1 - \frac{\bar{k}}{k_t^2 L} \sin \frac{k_t^2 L}{\bar{k}}\right) \Phi_n(k_t) \tag{3.3}$$

where $\bar{k}$ is the wave number of the incident radiation, and L is the length of the propagation path through the turbulence (5). Taking advantage of the rapid decay of the von Karman spectrum for $k_t > k_m$, Eq (3.3) can be approximated as

$$F_\varphi(k_t) \approx 2\pi \bar{k}^2 L \Phi_n(k_t) \tag{3.4}$$

where $\Phi_n(k_t)$ is defined as in Eq (3.1) and $\frac{k_m^2 L}{\bar{k}} << 1$. This assumption is satisfied for wavelengths near the visible spectrum and is typical of papers in this research area (5)(18)(8). Note that $F(k_t)$ defined in Eq (3.3) is different from $F_\varphi(k_t)$ defined in Eq (3.4). We use the φ subscript to indicate a phase spectrum derived from Eq (3.1), the von Karmen spectrum.

To develop an equivalent temporal spectrum, we assume that the structure of the inhomogeneities in the atmosphere remains fixed as it moves with the local wind velocity $\vec{v}$. The wind velocity is assumed to be perpendicular to the propagation direction of the wave front (Taylor's hypothesis of frozen turbulence). The single-sided temporal power spectrum of the incident wave front phase, $W(f)$, can be determined from:

$$W(f) = \frac{8\pi}{v} \int_0^\infty \mathrm{d}k_t \; F\left(\sqrt{k_t^2 + \left(\frac{2\pi f}{v}\right)^2}\right) \tag{3.5}$$

where the derivation of Eq (3.5) is presented in Appendix A. Substituting Eq (3.4) into the above expression:

$$W_\varphi(f) = \frac{8\pi}{v} \int_0^\infty \mathrm{d}k_t \frac{.033 C_n^2 2\pi \bar{k}^2 L}{\left(k_t^2 + \frac{4\pi^2 f^2}{v^2} + k_o^2\right)^{\frac{11}{6}}} e^{\frac{-k_t^2 + \frac{4\pi^2 f^2}{v^2}}{k_m^2}} \tag{3.6}$$

Letting $k_t^2 = \left(\frac{4\pi^2 f^2}{v^2} + k_o^2\right) x$ Eq (3.6) can be rewritten as

$$W_\varphi(f) = .033\left(\frac{2}{\pi^2}\right)^{\frac{1}{3}} C_n^2 \bar{k}^2 L v^{\frac{5}{3}} \left(f^2 + \frac{k_o^2 v^2}{4\pi^2}\right)^{\frac{-4}{3}} \int_0^\infty dx\, x^{\frac{1}{2}} (x+1)^{\frac{-11}{6}} e^{-\frac{x+1}{D^2}} \tag{3.7}$$

where $D = \frac{2\pi f}{k_m v}$. To make this function integrable in closed form it is necessary to omit the exponential term. This can be done if k_m is assumed to be large enough that the added high frequency power is small due to the remaining polynomial decay. Using the Beta function identity

$$\int_0^\infty dx \frac{x^{a-1}}{(x+1)^{a+b}} = \frac{\Gamma(a)\Gamma(b)}{\Gamma(a+b)} \tag{3.8}$$

the single-sided temporal power spectrum is finally written as

$$W_\varphi(f) = .033 C_n^2 \bar{k}^2 L v^{\frac{5}{3}} \left(f^2 + \frac{k_o^2 v^2}{4\pi^2}\right)^{\frac{-4}{3}} \tag{3.9}$$

3.2 Piston and tilt removed temporal power spectrum

In the previous section, we defined the temporal spectrum of phase fluctuations for a distorted wave front. Here, we go one step further and remove the power in the wave front associated with aperture piston and tilt. This is necessary because adaptive optical systems are insensitive to aperture piston. Additionally, most adaptive optical systems are designed to remove aperture tilt which accounts for between 80% and 90% of the variance of the distorted wave front (19)(14). By removing aperture piston and tilt from the input spectrum, we can better predict how well an adaptive optical system will correct higher order aberations as well as more accurately predict temporal response requirements.

The removal of aperture piston and tilt can be accomplished by using Eq (2.11) and the transfer function $T_\varphi(\vec{r})$ developed by Greenwood and Fried (GF). In order to use Eq (2.11) and avoid the problems associated with the use of the GF approximations to the phase difference power spectrum, $W_{\delta\varphi}(\vec{r}, f)$, discussed previously, it is necessary to first develop an expression for $W_{\delta\varphi}(\vec{r}, f)$ that accounts for the vectoral nature of $\vec{r}$. The vectoral

nature of $W_{\delta\varphi}(\vec{r}, f)$ can be accounted for by using an approach very similiar to that used by Tatarski to derive a relation equivalent to Eq (3.5) (18).

Following Tatarski's derivation,we start by writing the phase difference structure function:

$$D_{\delta\varphi}(\tau, \vec{r}) = \langle [\varphi(\vec{x}, t) - \varphi(\vec{x} + \vec{r}, t)] \times [\varphi(\vec{x} - \vec{v}\tau, t) - \varphi(\vec{x} + \vec{r} - \vec{v}\tau, t)] \rangle \tag{3.10}$$

where the two terms in brackets are the phase differences at two points separated by distance $\vec{r}$ at times t and $t + \tau$ and a frozen flow assumption has been made (18). Tatarski goes on to show that the identity

$$(a - b)(c - d) = \frac{1}{2}\left[(a - d)^2 + (b - c)^2 - (a - c)^2 - (b - d)^2\right] \tag{3.11}$$

can be used to convert Eq (3.10) to the more useful form:

$$D_{\delta\varphi}(\tau, \vec{r}) = \frac{1}{2}\left\{D_{\varphi}(\vec{r} - \vec{v}\tau) + D_{\varphi}(\vec{r} + \vec{v}\tau) - 2D_{\varphi}(\vec{v}\tau)\right\}. \tag{3.12}$$

where for a locally isotropic field $D_f(\vec{r}) = \langle [f(\vec{r} + \vec{r}') - f(\vec{r}')]^2 \rangle$.

Utilizing the Fourier transform relationship between $D_{\delta\varphi}(\tau, \vec{r})$ and $W_{\delta\varphi}(f, \vec{r})$,

$$D_{\delta\varphi}(\tau, \vec{r}) = 2\int_0^{\infty} \mathrm{d}f \, \cos(2\pi f\tau) \, W_{\delta\varphi}(f, \vec{r}), \tag{3.13}$$

and the relationship between $D_{\varphi}(\vec{r}, \vec{v}\tau)$, and $F_{\varphi}(k_t)$, given by Lee and Harp (12),

$$D_{\varphi}(\vec{r}, \vec{v}\tau) = 4\pi\int_0^{\infty} \mathrm{d}k_t \, k_t \left[1 - J_o(k_t |\vec{r} - \vec{v}\tau|)\right] F_{\varphi}(k_t) \tag{3.14}$$

and finally Eq (3.12), a relationship between $W_{\delta\varphi}(\vec{r}, f)$ and $F_\varphi(k_t)$ can be developed. The relation can be expressed as follows:

$$\begin{aligned} 2\int_0^\infty \mathrm{d}f' \cos(2\pi f'\tau)\, W_{\delta\varphi}(f', \vec{r}) &= \frac{1}{2}\Big\{4\pi\int_0^\infty \mathrm{d}k_t\, k_t\,[1 - J_o(k_t\,|\vec{r} - \vec{v}\tau|)]\, F_\varphi(k_t) \\ &\quad + 4\pi\int_0^\infty \mathrm{d}k_t\, k_t\,[1 - J_o(k_t\,|\vec{r} + \vec{v}\tau|)]\, F_\varphi(k_t) \\ &\quad - 8\pi\int_0^\infty \mathrm{d}k_t\, k_t\,[1 - J_o(k_t v\tau)]\, F_\varphi(k_t)\Big\} \end{aligned} \tag{3.15}$$

where $D_\varphi(\vec{x}) = D_\varphi(x)$ has been assumed. Assigning the wind velocity a particular direction, say the positive $\vec{x}$ direction, results in $|\vec{r} - \vec{v}\tau| = \sqrt{r^2 + v^2\tau^2 - 2rv\tau\cos\theta}$ and $|\vec{r} + \vec{v}\tau| = \sqrt{r^2 + v^2\tau^2 + 2rv\tau\cos\theta}$, where θ is the angle between $\vec{r}$ and the x-axis. Eq (3.15) can be simplified and expressed in the following form:

$$\begin{aligned} 2\int_0^\infty \mathrm{d}f' \cos(2\pi f'\tau)\, W_{\delta\varphi}(f', \vec{r}) &= 2\pi\int_0^\infty \mathrm{d}k_t\, k_t F_\varphi(k_t) \times \\ &\quad [2J_o(k_t v\tau) - J_o(k_t\,|\vec{r} - \vec{v}\tau|) - J_o(k_t\,|\vec{r} + \vec{v}\tau|)] \end{aligned} \tag{3.16}$$

Eq (3.16) can be further simplified by Fourier transforming it with respect to τ. Using the following relationship:

$$\int_{-\infty}^\infty \mathrm{d}\tau\, e^{j2\pi f\tau}\cos(2\pi f'\tau) = \frac{1}{2}[\delta(f + f') + \delta(f - f')] \tag{3.17}$$

the left hand side of Eq (3.16) is shown to equal

$$\int_0^\infty \mathrm{d}f'\ [\delta(f + f') + \delta(f - f')]\, W_{\delta\varphi}(f', \vec{r}) = W_{\delta\varphi}(f, \vec{r})\,. \tag{3.18}$$

Finally, the relation between $W_{\delta\varphi}(\vec{r}, f)$ and $F_\varphi(k_t)$ can be expressed as:

$$\begin{aligned} W_{\delta\varphi}(f, \vec{r}) &= 4\pi\int_0^\infty \mathrm{d}k_t\, k_t F_\varphi(k_t)\int_0^\infty \mathrm{d}\tau\, \cos(2\pi f\tau) \times \\ &\quad [2J_o(k_t v\tau) - J_o(k_t\,|\vec{r} - \vec{v}\tau|) - J_o(k_t\,|\vec{r} + \vec{v}\tau|)] \end{aligned} \tag{3.19}$$

where the evenness of the argument in τ has been exploited to simplify the integral. Although the derivation of the phase difference spectrum is not provided in their paper, GF's approximation of the above spectrum can be realized by setting θ to zero and performing the integrations. Setting $\theta = 0$ is equivalent to assuming that $\vec{r}$ and $\vec{v}$ are colinear over the integration of Eq (2.11). It should be clear at this point that such an assumption is clearly invalid.

Having determined the proper form of $W_{\delta\varphi}(f)$, we can proceed to evaluate the single-sided piston and tilt removed spectrum, $W_{\tilde{\varphi}}(f)$, using the GF method outlined in Chapter II. Recall Eq (2.11):

$$W_{\tilde{\varphi}}(f) = -\frac{1}{2}\int \mathrm{d}\vec{r}\; W_{\delta\varphi}(\vec{r}, f)\, T_{\varphi}(\vec{r})\,. \tag{3.20}$$

Substituting in $W_{\delta\varphi}(f)$ given in Eq (3.19), the complete integral form of the piston and tilt removed spectrum is

$$\begin{aligned} W_{\tilde{\varphi}}(f) \;=\; & -\frac{1}{2}\int \mathrm{d}\vec{r}\; 4\pi \int_0^{\infty} \mathrm{d}k_t\, \frac{.033 C_n^2 k_t 2\pi \bar{k}^2 L}{\left(k_t^2 + k_o^2\right)^{\frac{11}{6}}} e^{\frac{-k_t^2}{k_m^2}} \int_0^{\infty} \mathrm{d}\tau\, \cos(2\pi f\tau) \times \\ & \left[2J_o(k_t v\tau) - J_o(k_t|\vec{r} - \vec{v}\tau|) - J_o(k_t|\vec{r} + \vec{v}\tau|)\right] T_{\varphi}(\vec{r})\,. \end{aligned} \tag{3.21}$$

By making some convenient variable substitutions and interchanging the order of integration we arrive at a form which simplifies the numerical integration process:

$$\begin{aligned} W_{\tilde{\varphi}}(f) \;=\; & 3.04 D^2 \left(\frac{D}{v}\right) \left(\frac{r_o}{D}\right)^{-\frac{5}{3}} \times \\ & \int_0^{\infty} \mathrm{d}t\, \cos(2\pi f_o t) \int_0^{1} \mathrm{d}x\; x \int_0^{2\pi} \mathrm{d}\theta\; T_{\varphi}(x,\theta) \int_0^{\infty} \mathrm{d}k\, \frac{k\, e^{\left(\frac{-C_1 k}{2\pi C_2}\right)^2}}{\left(k^2 + \left(\frac{2\pi}{C_1}\right)^2\right)^{\frac{11}{6}}} \times \\ & \left[J_o\left(k\sqrt{x^2 + t^2 + 2xt\cos\theta}\right) + J_o\left(k\sqrt{x^2 + t^2 - 2xt\cos\theta}\right) - 2J_o(kt)\right]. \end{aligned} \tag{3.22}$$

where $f_o = \frac{fD}{v}$, $k = Dk_t$, $t = \frac{\tau v}{D}$, $C_1 = \frac{L_o}{D}$, and $C_2 = \frac{L_o}{l_o}$. By identifying the Fourier integral in Eq (3.22), we can also define the piston and tilt removed covariance as:

$$C_{\tilde{\varphi}}(\tau) = 1.54D^2\left(\frac{r_o}{D}\right)^{-\frac{5}{3}}\int_0^1 \mathrm{d}x\, x\int_0^{2\pi}\mathrm{d}\theta\; T_\varphi(x,\theta)\int_0^\infty \mathrm{d}k\, \frac{k\, e^{\left(\frac{-C_1 k}{2\pi C_2}\right)^2}}{\left(k^2+\left(\frac{2\pi}{C_1}\right)^2\right)^{\frac{11}{6}}}\times$$
$$\left[J_o\left(k\sqrt{x^2+t^2+2xt\cos\theta}\right)+J_o\left(k\sqrt{x^2+t^2-2xt\cos\theta}\right)-2J_o(kt)\right] \quad (3.23)$$

where $t = \frac{\tau v}{D}$. Recall, we have made the following assumptions to arrive at these equations: plane wave input, frozen flow turbulence, and single layer atmospheric turbulance. The form of this spectrum and its numerical evaluation will be discussed in Chapter IV.

3.3 Temporal equivalent spatial filter

Recall from Chapter I our model of the adaptive optical system mean square error:

$$\sigma^2 = \int_{-\infty}^{\infty}\mathrm{d}f\;|1-H(f)|^2 W(f) \quad (3.24)$$

where $W(f)$ is the temporal power spectrum of the wave front phase fluctuations due to atmospheric turbulence and $H(f)$ is the transer function of the adaptive optical system. In sections 3.1 and 3.2, we derived the temporal wave front spectra $W_{\tilde{\varphi}}(f)$ and $W_\varphi(f)$. Both of the temporal spectra can be used in Eq (3.24) to determine the residual wave front error. We can determine the effect of aperture piston and tilt removal on σ^2 by comparing the results of Eq (3.24) evaluated for $W_\varphi(f)$ and $W_{\tilde{\varphi}}(f)$. In order to make this calculation we also need to define the system transfer function $H(f)$.

Notice that $W_\varphi(f)$, $W_{\tilde{\varphi}}(f)$, and $H(f)$ are all functions of the temporal frequency variable f. We define $H(f) = H_S(f)\cdot H_T(f)$, where, as stated in Chapter I, $H_S(f)$ accounts for the spatial frequency response of the deformable mirror and $H_T(f)$ is the temporal transfer function. We have assumed that the spatial and

temporal transfer functions of the system are independent. This is reasonable if the computation time of the actuator weighting functions is insignificant compared to the integration time of the wave front sensor.

In order to come up with an expression for $H_S(f)$ based on the spatial frequency response of the deformable mirror we define a spatial transfer function $\tilde{H}_S(k_t)$ that accounts for the spatial wave front correction characteristics of the system. In section 3.1 we derived the temporal spectrum, $W_\varphi(f)$, from the spatial spectrum $F_\varphi(k_t)$ using relations developed in Appendix A (see Eq (3.5)). Using these same relations, it is possible to spatially filter $F_\varphi(k_t)$ to account for the spatial response characteristics of the deformable mirror and then convert the result to a temporal equivalent spectrum, $W_S(f)$. In other words, the spatial spectra of the deformable mirror surface is modeled as $F_S(k_t) = F_\varphi(k_t) \cdot \tilde{H}_S(k_t)$. Recall that, Eq (3.24) defines the spectral power difference between the incident wave front phase spectrum and the spectrum of corrector motion of the deformable mirror surface (see Fig 1.2). Using Eq (3.5), we can write the temporal equivalent spectrum, $W_S(f)$ as:

$$W_S(f) = \frac{8\pi}{v} \int_0^\infty \mathrm{d}\kappa_t \; F_S\left(\sqrt{\kappa_t^2 + \left(\frac{2\pi f}{v}\right)^2}\right). \tag{3.25}$$

Finally, the temporal equivalent filter $H_S(f)$ is equated to:

$$H_S(f) = \sqrt{\frac{W_S(f)}{W_\varphi(f)}}. \tag{3.26}$$

This approach is relatively simple if we know the form of the two dimensional spatial phase spectrum, $F(k_t)$. Eq (3.4) describes $F_\varphi(k_t)$, the spatial frequency equivalent of $W_\varphi(f)$ Unfortunately, we do not yet have a spatial frequency representation, $F_{\tilde{\varphi}}(k_t)$, for the aperture piston and tilt removed spectrum $W_{\tilde{\varphi}}(f)$. Because $W_{\tilde{\varphi}}(f)$ varies for each point on the aperture, the random process described by $W_{\tilde{\varphi}}(f)$ is not WSS in the spatial domain, and as such, $F_{\tilde{\varphi}}(k_t)$ does not exist. We recognize the requirement of stationarity when using linear systems approaches, and therefore assume local stationarity over a subaperture centered at the point of interest. This assumption approaches validity as the subaperture size decreases and is necessary if a linear systems

approach in the frequency domain is to be used. Most important, this assumption allows us to hypothesize the exitance of the aperture piston and tilt removed spatial frequency dependent spectrum $F_{\tilde{\varphi}}(k_t)$.

In order to determine the effect of $\tilde{H}_S(k_t)$ on a piston and tilt removed spectrum, we must first determine $F_{\tilde{\varphi}}(k_t)$. To this point we have been using Eq (3.5) to transform a spatially dependent spectrum to a temporally dependent spectrum. Here, we postulate that it is possible to perform the inverse operation and determine $F_{\tilde{\varphi}}(k_t)$ given $W_{\tilde{\varphi}}(f)$. In Appendix A, we determine the inverse of Eq (3.5) to be:

$$F(k_t) = -\int \mathrm{d}k_z \, \frac{v^2}{8\pi^3 k} W'\left(\frac{v\sqrt{k_t^2 + k_z^2}}{2\pi}\right). \tag{3.27}$$

With this last relation, we can determine $F_{\tilde{\varphi}}(k_t)$, and proceed to spatially filter this spectrum for a given system spatial response, $F_S(k_t) = F_{\tilde{\varphi}}(k_t) \cdot \tilde{H}_S(k_t)$. Eqs (3.25) and (3.26) can then be used to determine the temporal equivalent filter $H_S(f)$, and finally the residual error of our adaptive optical system is found by applying Eq (3.24).

3.4 Summary

In this chapter we developed the mathematical methods needed to model the performance of an adaptive optical system in the frequency domain. Section 3.1 developed a description of the spectrum of atmospheric turbulence induced phase fluctuations. Section 3.2 developed an integral representation of the same spectrum that accounted for piston and tilt removal across an aperture. Finally, in section 3.3, we developed the mathematical transformations necessary to account for the temporal equivalent spatial response of a system. Fig 3.1 descibes the process developed in this chapter pictorally. In the following chapter, these methods are used to determine system performance for several spatial and temporal transfer functions.

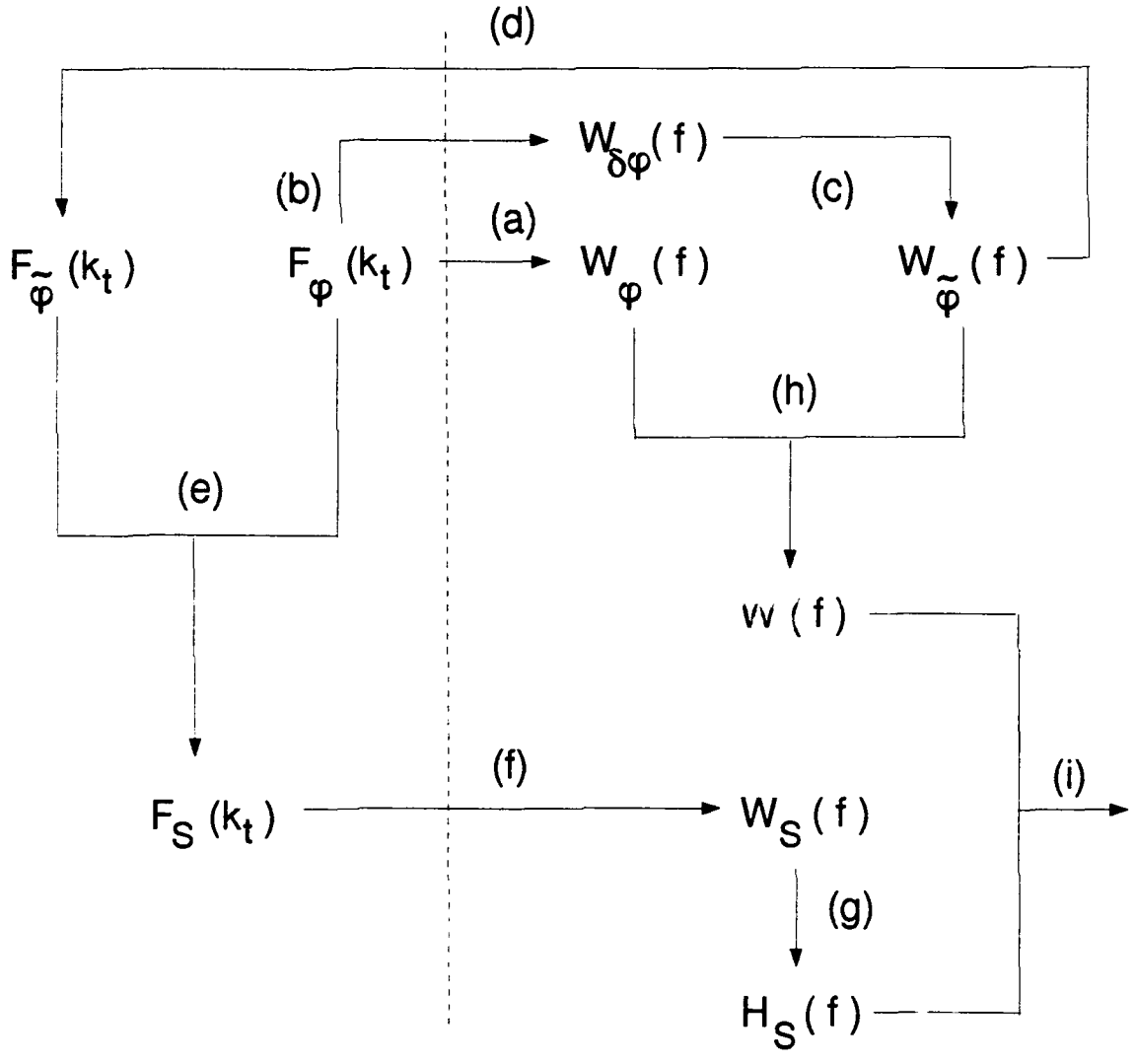

Figure 3.1. Flow diagram of the frequency domain approach used to determine system performance. (a) 2-D spatial spectrum to equivalent temporal spectrum, Eq (3.5); (b) 2 D spatial spectrum to phase diffrence spectrum, Eq (3.19); (c) GF transform accounting for piston and tilt removal, Eq (2.11); (d) determination of the locally stationary piston and tilt removed spatial spectrum, Eq (3.27); (e) $F_S(k_t) = F_\varphi(k_t) \cdot \tilde{H}_S(k_t)$; (f) 2-D filtered spatial spectrum to equivalent temporal spectrum, Eq (3.5); (g) determination of the temporal equivalent spatial transfer function, Eq (2.11); (h) spectrum of incident wavefront phase (i) determination of residual error, Eq (3.24).

IV. Numerical Results

In this chapter we apply the methods developed in the previous chapters to determine the performance of a theoretical adaptive optical system. Before obtaining results for system performance however, it is still necessary to determine numerically the form of $W_{\tilde{\varphi}}(f)$. Recall that $W_{\tilde{\varphi}}(f)$ is the piston and tilt removed temporal spectrum for a single point in the aperture. These calculations are very time intensive and only few representative points on the aperture will be evaluated. Section 4.1 details these calculations and presents plots of $W_{\tilde{\varphi}}(f)$. In section 4.2, we assume forms for both $\tilde{H}_S(k_t)$ and $H_T(f)$. Recall, $\tilde{H}_S(k_t)$ accounts for the spatial response characteristics of the deformable mirror and $H_T(f)$ for the temporal characteristics of the control loop. In section 4.3, we evaluate Eq (3.24) to determine the residual wave front error as a function of system response time. These results are presented along side those of Fried and Karr for comparison (2)(11).

4.1 Calculation of the piston and tilt removed spectrum

To numerically evaluate the piston and tilt removed covariances and spectra, $C_{\tilde{\varphi}}(\tau)$ and $W_{\tilde{\varphi}}(f)$, for single points across an aperture, we must define the following constants: C_1, C_2, and $\vec{r}_1$. Recall, $C_1 = \frac{L_o}{D}$, and $C_2 = \frac{L_o}{l_o}$ and $\vec{r}_1$ describes the location of the subaperture in the overall aperture. Because of the difficulty and time involved in evaluating Eqs (3.22) and (3.23), we define a limited number of $\vec{r}_1$ positions on the aperture. We will evaluate only the covariances and spectra for $\frac{r_1}{D} = 0.0, 0.225$, and 0.45 where the radial distances have been chosen to lie in a line along the same vector direction as the wind. It is expected that, the power of the temporal wave front fluctuations will be at a maximum along this line.

Although many different values are quoted for the size of the outer scale, Coulman et. al. find that L_o has an upper limit of about 5 meters for problems associated with astronomical seeing (1). From Goodman, the inner scale size, l_o, is on the order of about a millimeter (5). Using this information, we determine C_2 to be on the order of 4000. The spectral power at frequencies on the order of $(l_o)^{-1}$ is very small making our analysis insensitive to small error in estimating C_2. This ratio will thus be held constant throughout our calculations.

Fig 4.1 illustrates the effect of piston and tilt removal on the reference input spectrum. Note that the power in the piston and tilt removed spectra increases as the magnitude of the radial position $\vec{r}_1$ increases. This is due to the higher variance of the tilt correction as the measurment is taken closer to the edge of the aperture. Also note that piston and tilt correction is effective up to temporal frequencies on the order of $\frac{v}{D}$. For temporal frequencies greater than $\frac{v}{D}$ the curves have the familiar $f^{-8/3}$ slopeand the input and piston and tilt removed spectra have the same power. Equivalently, we can determine that piston and tilt correction is effective for spatial frequencies up to $\frac{1}{D}$ using the fact that $f = \frac{k_t v}{2\pi}$, (see Appendix A).

The parameter $C_1 = \frac{L_o}{D}$ was chosen to equal 2π. This value was chosen so that D would be on the order of two-thirds meters for $L_o = 4$. This has significance because we can compare our theoretical low frequency data to that collected experimentally by Greenwood for an aperture of $D = 0.6$ meters (7). Greenwood's xperimental data plot depicts the same flattening in the low frequency portion of the spectrum as shown in Fig 4.1 for $r_1 = 0.0$. This flattening occurs at a value of about 10^{-2} waves^{2}Hz^{-1} experimentally as compared with our theoretical value of 0.013 waves^{2}Hz^{-1}. This agreement between the experimental and theoretical data gives us confidence in our spectrum modeling methodology. Comparing the spectra of Greenwood and Fried described in Chapter II to those of Fig 4.1, we find that accounting for the vectoral nature of $W_{\delta\varphi}(\vec{r}, f)$ has a significant effect for low frequencies and and none for frequencies following the $f^{-8/3}$ asymtote. Recall from Chapter II, the GF piston and tilt removed spectra follow an $f^{4/3}$ asymtote for temporal frequencies less than $\frac{v}{D}$.

In Fig 4.2, we allow the aperture size to increase to that of the outer scale so that $C_1 = \frac{L_o}{D} = 1$. This figure shows that aperture piston and tilt correction are not as effective at removing phase distortions when the aperture size becomes large relative to the outer scale. When the period of a particular spatial frequency is less than the aperture size it is unaffected by piston and tilt correction. Thus as the aperture grows larger, the power in correspondingly lower spatial frequencies remains unaffected by aperture piston and tilt correction. In Fig 4.1, piston and tilt correction removes over 90% of the of the spectral power present in the reference wave front at $r_1 = 0.0$; whereas, only 33% of the spectral power is removed in Fig 4.2. When comparing the spectra of Figs 4.1 and 4.2, it is important to remember that the power is scaled by the size of the aperture. Taking D into

account, the input spectra of both figures have the same value. Realizing this, it is clear that a smaller percentage of the input power spectra is removed in as D approaches L_o.

4.2 System performance

In this section, we specify the transfer functions, $H(f)$, used to represent the the spatio-temporal response characteristics of several adaptive optical systems. Recall that $H(f) = H_S(f) \cdot H_T(f)$ and that $H_S(f)$ is determined from $\tilde{H}_S(k_t)$ using methods outlined in ChapterIII. The spatial transfer function, $\tilde{H}_S(k_t)$, is defined in subsection 4.2.1 and the temporal transfer function, $H_T(f)$, in subsection 4.2.2.

4.2.1 Spatial filter. A deformable mirror's spatial transfer function, $\tilde{H}_S(k_t)$, can be characterized by the size of its subapertures for a segmented type of device or by the distance between actuators and the actuator influence function for continuous surface type device (13)(19)(10). In this investigation, we idealize the performance of the adaptive optical system's deformable mirror by approximating its spatial frequency performance to be:

$$\tilde{H}_S(k_t) = \begin{cases} 1, & |k_t| \leq \frac{\pi}{d} \\ 0, & |k_t| > \frac{\pi}{d}. \end{cases} \tag{4.1}$$

where d is the diameter of the deformable mirror's subapertures. This estimate of deformable mirror performance is consistant with Nyquist sampling rates and has been chosen for simplicity. Additinally, Tyson finds that spatial filtering models essentially the same as Eq (4.1) are adequate for characterizing the performance of adaptive optical systems (19). This filter choice also helps us avoid the issue of a nonstationary $\varphi(t)$. Recall, it is the inherent piston and tilt removal of the adaptive optical system that causes $\varphi(t)$ to be non-stationary. Because piston and tilt removal only affects spatial frequencies below $k_t = \frac{2\pi}{D}$, we can consider those above $k_t = \frac{2\pi}{D}$ to be stationary. Because our chosen $\tilde{H}_S(k_t)$ only affects frequencies greater than $k_t = \frac{2\pi}{D}$, we consider our linear systems approach to be valid.

At this point, we are ready to determine the temporal equivalent transfer function $H_S(f)$. Using the methods described in section 3.3, we could determine $F_\varphi(k_t)$ and $F_{\tilde{\varphi}}(k_t)$ for the spectra plotted in Fig 4.1,

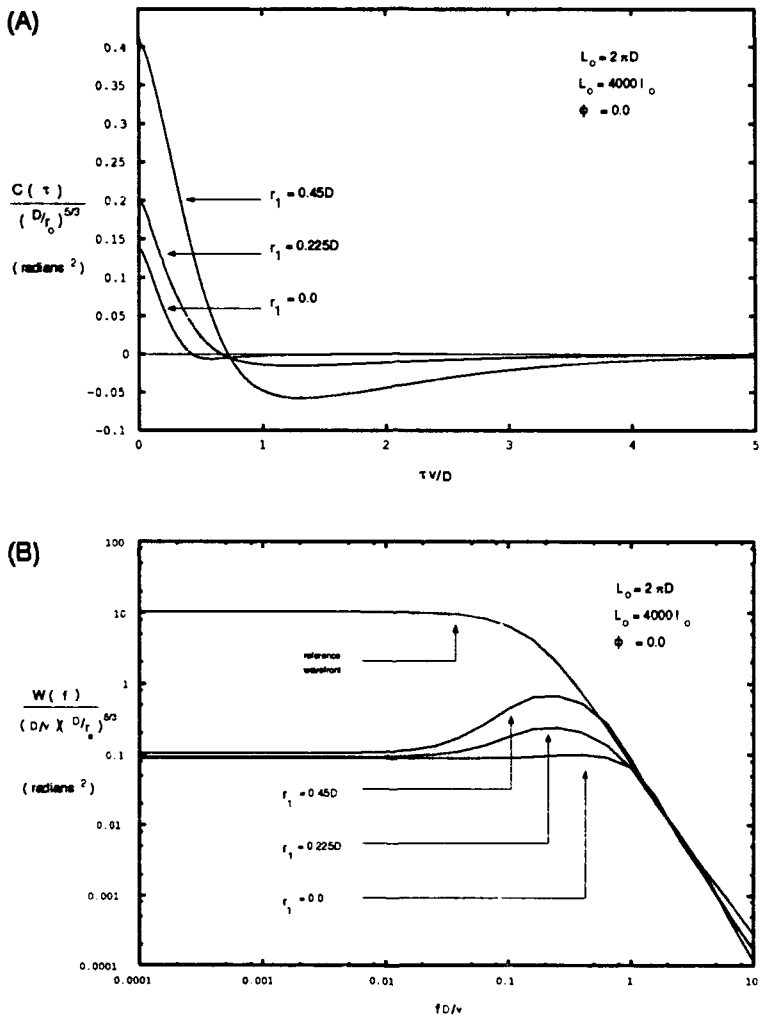

Figure 4.1. Temporal (A) covariances, $C_{\tilde{\varphi}}$, and (B) spectra, W_{φ} and $W_{\tilde{\varphi}}$, of wave front phase fluctuations for the case of $\frac{L_o}{D} = 2\pi$. The piston and tilt removed spectrum, $W_{\tilde{\varphi}}$, has been evaluated at $|\vec{r}_1| = 0.0$, $0.225D$, and $0.45D$ along the direction of the wind.

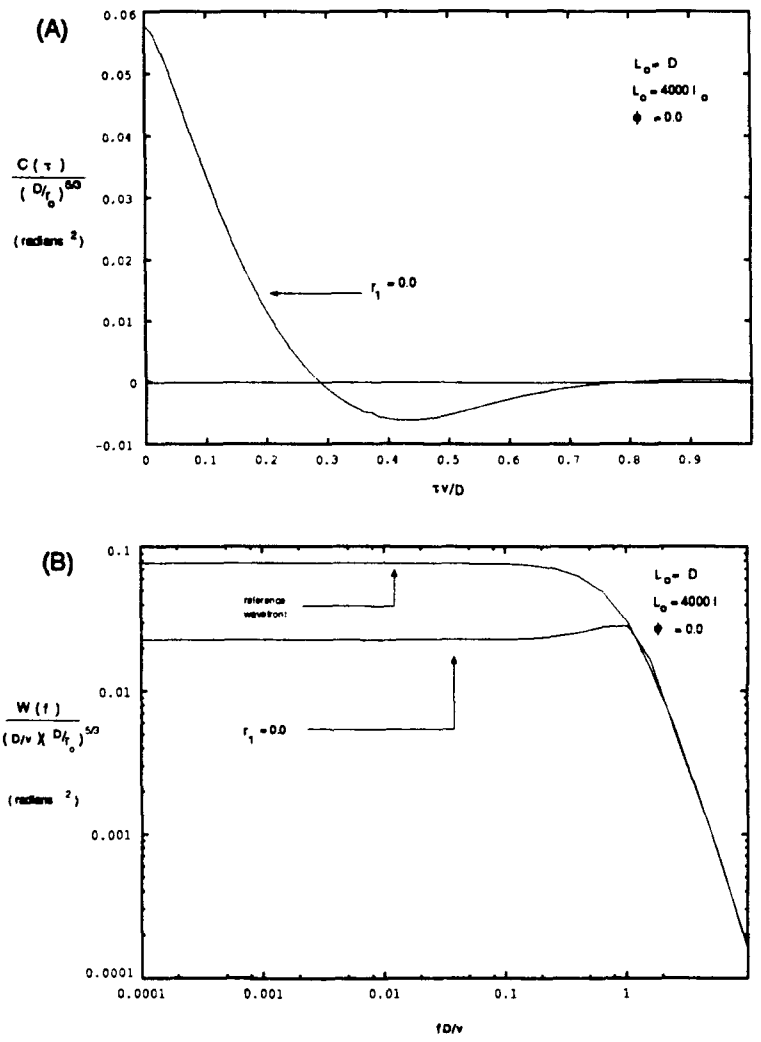

Figure 4.2. Temporal (A) covariances, $C_{\tilde{\varphi}}$, and (B) spectra, W_{φ} and $W_{\tilde{\varphi}}$, of wave front phase fluctuations for the case of $\frac{L_o}{D} = 1$. The piston and tilt removed spectrum, $W_{\tilde{\varphi}}$, has been evaluated for $\vec{r}_1 = 0.0$.

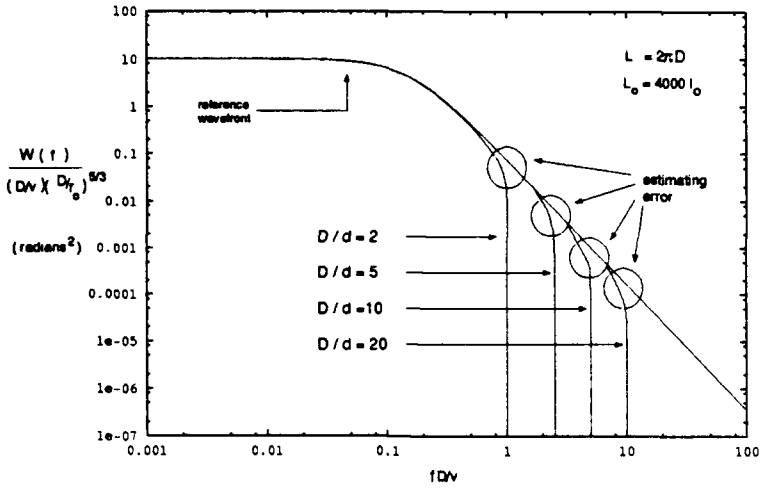

Figure 4.3.

Temporal equivalent spatially filtered spectrum $W_S(f)$ depicting the effect of $\tilde{H}_S(k_t) = \text{rect}\left(\frac{k_t d}{\pi}\right)$ for $\frac{D}{d} = 2, 5, 10,$ and 20. The circled error is the difference between $W_S(f)$ and our approximation of the spatial filtering effect, $\text{rect}\left(\frac{f2D}{Xv}\right) \cdot W_\varphi(f)$.

multiply by $\tilde{H}_S(k_t)$, and determine $H_S(f)$ using Eqs (3.25) and (3.26). Instead, we choose to simplify this procedure and model the temporal equivalent spatial filtering by

$$H_S(f) \approx \begin{cases} 1, & |f| \leq \frac{Xv}{2D} \\ 0, & |f| > \frac{Xv}{2D}. \end{cases} \tag{4.2}$$

where $X = \frac{D}{d}$. The spatial cutoff point of $H_S(f)$ is determined from $f = \frac{k_t v}{2\pi}$, (established in Appendix A). Fig 4.3 shows this to be a reasonable approximation for a representative number of $\frac{D}{d}$ values.

To make a gross estimate of the maximum error involved in approximating $H_S(f)$ by Eq (4.2), we note from Appendix A:

$$W(f) = \frac{4\pi}{v} \int_{\frac{2\pi|f|}{v}}^{\infty} \frac{d\kappa\, \kappa F(\kappa)}{\left(\kappa^2 - \left(\frac{2\pi f}{v}\right)^2\right)^{1/2}}. \tag{4.3}$$

From Eq (4.3), we can deduce that the spectral power at any temporal frequency f is the weighted sum of the spatial frequencies equal to or above $\kappa_t = \frac{2\pi f}{v}$. Because the spatial filter described by Eq (4.1) rejects frequencies above some $k_{c.o.} = \frac{\pi}{d}$, all temporal frequencies will suffer a loss in spectral power associated with

the spatial frequency band from $k_{c.o.}$ to infinity. Additionally, since the weighting of these spatial frequencies is greatest for $f_{c.o.}$, $\frac{k_{c.o.}v}{2\pi}$, we can quantify the approximation error over all temporal frequencies, from 0 to $f_{c.o.}$, as $W(f_{c.o.}) \times f_{c.o.}$. From Fig 4.1 and Eq (3.9), we determine that $W(f_{c.o.}) = (f_{c.o.})^{-\frac{8}{3}}$. A conservative estimate of the maximum error involved in assuming $H_S(f)$ has the form of Eq (4.2) is $(f_{c.o.})^{-\frac{5}{3}}$.

4.2.2 Temporal filter. To characterize the temporal response of our theoretical adaptive optical system, we assume that the dominant delay in the actuator control loop is the integration time of the wave front sensor. An intuitive linear systems approximation of this integration process is given by the following temporal impulse response:

$$h_T(t) = \text{rect}\left(\frac{t-\tau}{2\tau}\right). \tag{4.4}$$

Where τ is the average delay between wave front sensing and actuator positioning and 2τ is the length of the wave front sensor integration. In the Fourier domain, we can write Eq (4.4) as

$$H_T(f) = \text{sinc}(2\pi f\tau)e^{-j2\pi f\tau}. \tag{4.5}$$

The phase delay term in $H_T(f)$ accounts for the decorrelation between the sensed wave front and the corrected wave front; while, the sinc term limits the temporal bandwidth of the wave front sensor simulating the smoothing effect of the integration process.

4.3 Calculation of residual error

In this section, we will use Eq (3.24) to model the residual error of adaptive optical systems descibed by the spatial and temporal transfer functions of section 4.2. The temporal frequency spectra of Fig 4.1 will be used as the input spectra, $W(f)$, to Eq (3.24). These spectra include three that account for aperture piston and tilt removal, $W_{\tilde{\varphi}}(f)$, for points located at radial distances $r_1 = 0.0, 0.225D$, and $0.45D$ along the direction of $\vec{v}$ and one that assumes no piston or tilt correction, $W_{\varphi}(f)$. All plots of system performance depict wave front error measured in waves versus time delay of the system. The wave front error has been normalized by $\left(\frac{D}{r_o}\right)^{\frac{5}{6}}$

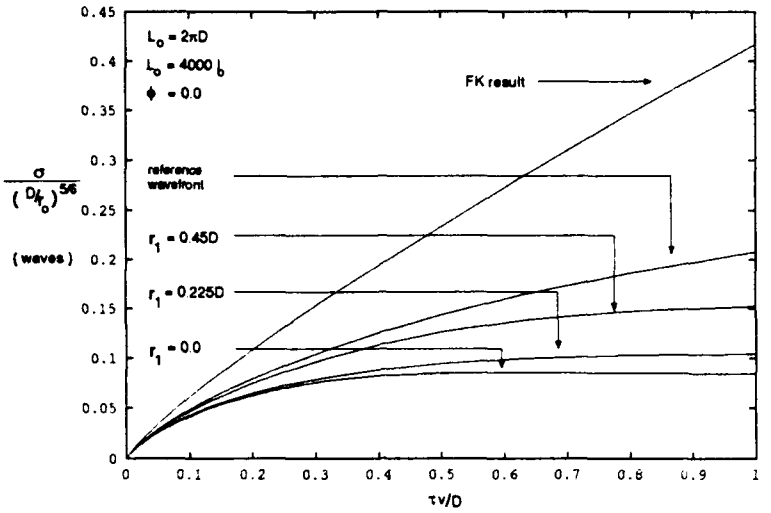

Figure 4.4. Residual wave front error due to finite system delay, ($|H(f)| = 1$).

and the time delay, τ, has been normalized by $\frac{D}{v}$. We are now ready to evaluate Eq (3.24) numerically and determine the performance of our system.

4.3.1 The effect of phase delay. In Fig 4.4, $H(f)$ has been simplified to account only for the temporal delay of the system, $H_T(f) = e^{-j2\pi f\tau}$ and $|H(f)| = 1$. This models the case of perfect spatial wave front correction, $d = 0$ for the deformable mirror subaperture size, and neglects the effects of temporal bandwidth limitations caused by the integration process of the wave front sensor. We model this simple case so that the individual effects of spatial and temporal bandwidth limitations and temporal delay can be distinguished in later plots. The curves of Fig 4.4 plot wave front error for five different cases. The three lower curves are for the piston and tilt removed input spectra $W_{\tilde{\varphi}}(f)$. The upper two curves assume no piston or tilt correction. The lower of these last two is for the input spectrum $W_{\varphi}(f)$ derived in section 3.1. Recall, $W_{\varphi}(f)$ was derived assuming a von Karmen index of refraction fluctuation power spectrum. The uppermost curve is a plot of the FK result, (see Eq (1.1). FK assumed a Kolmogorov index of refraction fluctuation power spectrum. The FK result can be written in closed form as

$$\sigma^2 = 6.885 \left(\frac{v\tau}{D}\right)^{\frac{5}{3}} \left(\frac{D}{r_o}\right)^{\frac{5}{3}} \tag{4.6}$$

where Eq (1.1) has been rewritten in terms of r_o . For a plane wave propagating through a single turbulence layer, the Greenwood frequency in Eq (1.1) can be expressed as $f_G = 0.4277\frac{v}{r_o}$ (6)(20).

We can make several observations concerning Fig 4.4. First, the error described by the curves for $r_1 = 0.0, 0.225D$, and $0.45D$ and the reference wave front seems to approach some limiting error as the time delay increases. This is due to the sensed wave front becoming uncorrelated with the incoming wave front as the time between sensing and correction increases. The small increase in error as delay time gets longer is due to the finite power, (see Fig 4.1), at very low frequencies in both $W_\varphi(f)$ and $W_{\tilde{\varphi}}(f)$. The upper limit on the error is equal to twice the power under the respective spectrum. Second, the error described by the FK result is higher than that for the piston and tilt included reference wave front, $W_\varphi(f)$. This is due to the FK assumption of a Kolmogorov spectrum which has power approaching infinity at low temporal frequencies whereas our assumption of a von Karmen spectrum limits the power in $W_\varphi(f)$ to finite values at all frequencies. The large increase in error as delay time gets longer for the FK result is due to the infinite power at very low frequencies of the Kolmogorov spectrum.

4.3.2 The effect of limited temporal bandwidth. In Fig 4.5 we include the effect of the integration process to the phase delay effects depicted in Fig 4.4. As stated previously, the integration process of the wave front sensor affects the bandwidth of $H_T(f)$. Fig 4.5 still assumes the case of infinite spatial bandwidth, $H_S(f) = 1$. As the integration time of the wave front sensor becomes longer, the temporal bandwidth of $H_T(f)$ becomes smaller. This decrease in the temporal bandwidth of $H_T(f)$ is best evidenced for long time delays and is negligble for very small τ due to the small amount of power in $W_\varphi(f)$ at high frequencies. As τ becomes large, the rms error of Fig 4.4 is equal to approximately $\sqrt{2}$ times the rms error of Fig 4.5. This difference occurs because the sensed wave front and the corrected wave front become uncorrelated as the time between sensing and correction increases. This loss of correlation for large τ results in $\sigma^2 = \sigma^2_{sensed} + \sigma^2_{corrected}$ where $\sigma^2_{sensed} \approx \sigma^2_{corrected}$ for $|H_T(f)| = 1$. For the case of the bandwidth limited transfer function, $|H_T(f)| = \text{sinc}(2\pi f\tau)$, σ^2_{sensed} approaches zero for large τ. Notice that Figs 4.4 and 4.5 are plotted for σ and not σ^2. The difference between the two plots for a specific curve will thus be $\sqrt{2}$.

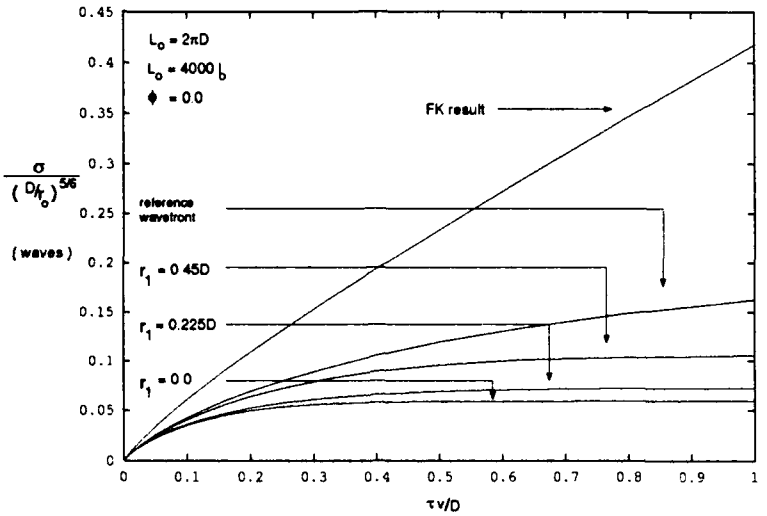

Figure 4.5. Residual wave front error for system temporal response $H_T(f)$ where $|H_S(f)| = 1$.

4.3.3 The effect of subaperture size. Figs 4.6 and 4.7 account for the spatial bandwidth limitations of the deformable mirror in addition to the effects of the system temporal response described in subsections 4.3.1 and 4.3.2. The temporal equivalent spatial bandwidth of $H_S(f)$ is related to subaperture size by Eq (4.2). Fig 4.6 depicts the effect of an aperture to subaperture size ratio of $\frac{D}{d} = 10$ on system performance. Comparing the curves of Fig 4.6 with those of Fig 4.5, we note that the subaperture size of the deformable mirror has little effect on the system for large τ. As the temporal response of the system becomes faster though, the finite size of the subapertures becomes the limiting factor of the system's wave front correction performance. For $\frac{D}{d} = 10$, Fig 4.6 shows the scaled error in waves to be just less than 0.01. Fig 4.7 shows that as the subaperture size grows larger the error also increases. For very limited correction, $\frac{D}{d} = 2$, the scaled error plotted in Fig 4.7 is approximately 0.033 waves.

From Fig 4.7, we can determine the slowest system response time that takes full advantage of our system's spatial response. This point will be located at the point on the curve where significant reduction in residual error is no longer achieved for faster response time. We will refer to this point as τ_{design}. Comparing our results with those of Fried and Karr, we find that the τ_{design} predicted by our study is similiar in magnitude to that of the FK result. The coincidence of our result and that of Fried and Karr becomes closer as we approach the FK

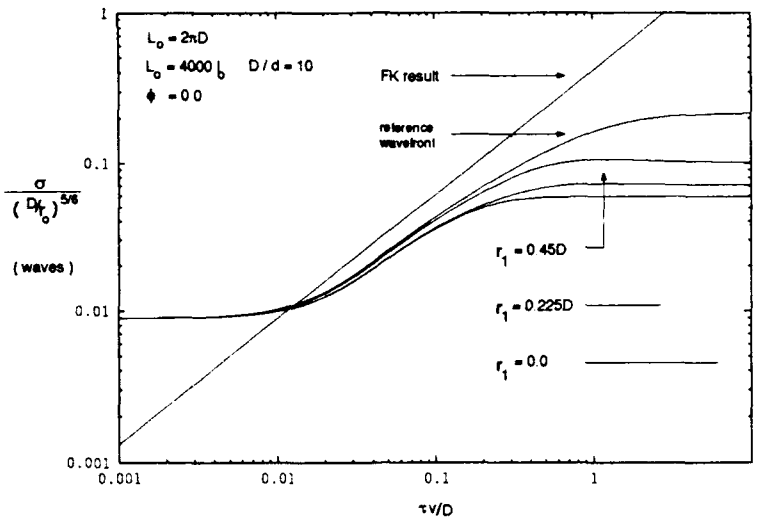

Figure 4.6. Residual wave front error for system response $H(f)$ for $\frac{D}{d} = 10$.

assumption of $\frac{D}{d} = \infty$. The largest discrepancies between the FK result and the results of this investigation will be for partial correction systems where $\frac{D}{d}$ is less than around five. Fig 4.7 shows that the FK predicted temporal response requirement is almost double our predicted requirement of $\tau_{design} \approx \frac{0.1D}{v}$ for $\frac{D}{d} = 2$. Thus, for partial correction systems, the FK result does not predict temporal response requirements as effectively as for higher order correcting systems.

From Figs 4.6 and 4.7, we also determine that accounting for piston and tilt removal is not necessary if we are interested in the area of the the curves near τ_{design}. Fig 4.7 shows that τ_{design} will always be less than $\approx \frac{0.1D}{v}$. Corresponding values of τ in Fig 4.6 show the difference between residual error for W_φ and for the three curves representing $W_{\tilde{\varphi}}$ is very small. This difference is greatest for the $W_{\tilde{\varphi}}$ curve representing the center of the aperture but would be less if we looked at an average $W_{\tilde{\varphi}}$ over the entire aperture. Recall, we only evaluated $W_{\tilde{\varphi}}$ at three points in the aperture, and that although the point at $(r_1 = 0.45D, \phi = 0)$ has the worst case spectrum, the point at the center, $r_1 = 0$, is best case.

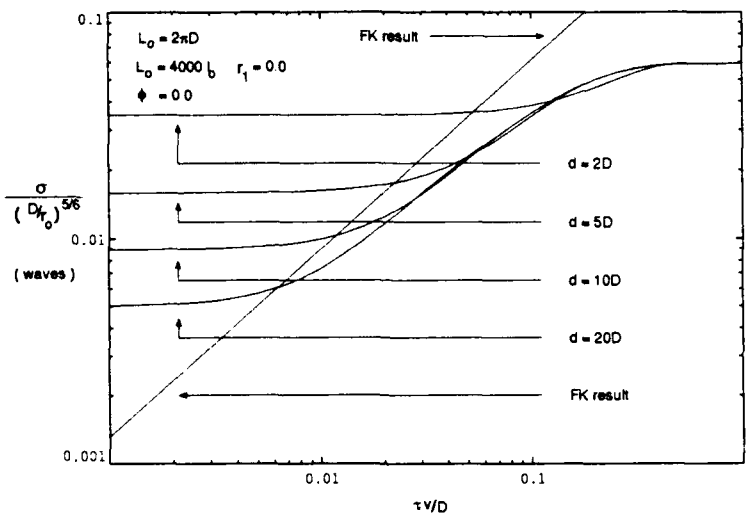

Figure 4.7. Residual wave front error due to system response at $r_1 = 0$.

4.4 Summary

In section 4.1 of this chapter we evaluated Eq (3.22) and determined the piston and tilt removed spectra for several values of the system charateristic constants C_1, C_2, and $\vec{r}_1$. The resulting spectra were found to be in agreement with experimentally gathered data, and also reflected expected performance trends of piston and tilt correction. In section 4.2 we defined the spatial and temporal response characteristics of several system transfer functions. Section 4.3 presented the rms residual error estimates for the previous section's system transfer functions. These estimates of system performance were found to predict a maximum control loop delay not greater than twice that predicted by the FK result. This agreement of our error predictions with those of Fried and Karr as well as the reflection of expected performance trends validates our results.

V. Conclusions

The primary objective of this investigation was to develop a frequency domain approach, using linear systems methods, that describes performance effects of an adaptive optical system's temporal response taking into account aperture piston and tilt removal and spatial bandwidth limitations due to finite subaperture size. We modeled system performance as the mean square residual phase error of the corrected wave front $\varphi_c(\vec{x}, t)$:

$$\sigma^2 = \int_{-\infty}^{\infty} \mathrm{d}f \ |1 - H(f)|^2 W(f). \tag{5.1}$$

In Chapter III, we developed spectral representations for the wave front incident on the deformable mirror, $W(f)$, and also for the system transfer function $H(f)$. The unique aspect of this model is the relative ease with which performance characteristics of different spatial and temporal system response functions can be investigated. Although methods were developed in section 3.3 to account for an arbitrary transfer function $H(f)$, section 4.2.1 introduced idealized temporal equivalent spatial transfer functions that greatly simplified the numerical evaluation process. Using these spatial filtering concepts, the effects of limited system spatial bandwidth can determined more efficiently than with those of GF. The simple multiplication involved in accounting for the temporal characteristics of a system make this model especially useful for comparing the performance of different temporal transfer functions.

The secondary objective was to address when use of our approach yields substantially different results than those of Fried and Karr. Section 4.3 shows that for τ greater than $\frac{D}{v}$ the FK result does not provide adequate modeling of system performance. However, response times of systems that take full advantage of of the deformable mirror spatial response are less $\frac{0.1D}{v}$. As stated in section 4.3, we call this temporal delay time τ_{design}. For a system with minimum spatial response, $\frac{D}{d} = 2$, the difference between the FK result and that predicted by our approach for τ_{design} is less than a factor of two. This agreement, in predicting the residual error for τ_{design} of our approach and that of Fried and Karr validates our results. Although the FK result is more easily evaluated, use of the methods developed in this thesis provide more insight into the performance trade-offs of systems having different temporal and spatial characteristics.

Additionally, we found that our approach could be significantly simplified if we were interested in response times less than $\frac{0.1D}{v}$, τ near τ_{design}. The most difficult part of our approach was developing the piston and tilt removed spectra and a method to spatially filter this spatially nonstationary spectra, and in section 4.3.3, we found that piston and tilt removal had little effect on the error predictions generated by our approach for response times less than $\frac{0.1D}{v}$. Thus, our approach becomes numerically more appealing while still providing the ability to compare different temporal and spatial parameters. This is especially relevant for the case of large apertures. As found in section 4.1, piston and tilt removal have significantly less effect on the spectra of phase fluctuations for aperture sizes aproaching the outer scale size of the atmosphere, L_o.

In summary, the objective of developing a frequency domain model of adaptive optical system performance has been met, and although the FK result adequately predicts the residual error for time delays of interest, our approach determines the value of the maximum time delay that sill takes full advantage of the spatial response of the deformable mirror.

Appendix A.

This appendix develops the methodology that will be used to transform a given temporal spectrum to an equivalent two dimensional spatial frequency spectrum and the reverse. Our development follows Tatarski's almost identical development for the three dimensional spatial spectrum (18).

We begin this development by defining the two dimensional spatial single dimension temporal correlation function by:

$$B(\vec{r},\tau) = \langle \varphi(\vec{x},t)\,\varphi(\vec{x}+\vec{r},t+\tau)\rangle \tag{A.1}$$

where $\varphi(\vec{x},t)$ is a WSS spatio-temporal random field and $\vec{r} = (\Delta x, \Delta y)$. Using Taylor's frozen flow assumption, the temporal changes in the field $\varphi(\vec{x},t)$ can be represented as simple spatial shifts:

$$\varphi(\vec{x},t+\tau) = \varphi(\vec{x}-\vec{v}\tau,t)\,. \tag{A.2}$$

where $\vec{v}$ repesents the magnitude and direction of the field flow. Substituting Eq (A.2) into Eq (A.1):

$$B(\vec{r},\tau) = B(\vec{r}-\vec{v}\tau) \tag{A.3}$$

The three dimensional spectrum of $B(\vec{r}-\vec{v}\tau)$ can be found through the Fourier transform relation:

$$u(\vec{\kappa},f) = \left(\frac{1}{2\pi}\right)^2 \iiint \mathrm{d}\vec{r}\,\mathrm{d}\tau\; e^{-j(\vec{\kappa}\cdot\vec{r}+2\pi f\tau)} B(\vec{r}-\vec{v}\tau) \tag{A.4}$$

Performing the spatial transform,

$$u(\vec{\kappa},f) = \int \mathrm{d}\tau\; e^{-j2\pi f\tau} e^{-j\vec{\kappa}\cdot\vec{v}\tau} F(\vec{\kappa}) \tag{A.5}$$

where $F(\vec{\kappa})$ represents the two dimensional spatial spectrum of the field $\varphi(\vec{x}, t)$. The important relation between the spatio-temporal spectrum and the spatial spectrum for a frozen flow field is found to be:

$$u(\vec{\kappa}, f) = \delta\left(f + \frac{\vec{\kappa} \cdot \vec{v}}{2\pi}\right) F(\vec{\kappa}). \tag{A.6}$$

By writing $B(\vec{r}, \tau)$ in terms of its Fourier transform,

$$B(\vec{r}, \tau) = \iiint \mathrm{d}\vec{\kappa}\, \mathrm{d}f\, e^{j(\vec{\kappa}\cdot\vec{r} + 2\pi f\tau)} u(\vec{\kappa}, f), \tag{A.7}$$

we can begin to develop a relationship between the temporal frequency spectrum,

$$W(f) = \int \mathrm{d}f\, e^{j2\pi f\tau} B(\tau), \tag{A.8}$$

and the two dimensional spatial spectrum, $F(\vec{k})$. Letting the spatial difference vector $\vec{r}$ in $B(\vec{r}, \tau)$ go to zero, the temporal covariance function can be written as:

$$B(0, \tau) = B(\tau) = \int \mathrm{d}f\, e^{j2\pi f\tau} \left[\iint \mathrm{d}\vec{\kappa}\, u(\vec{\kappa}, f)\right], \tag{A.9}$$

and the relation between the temporal spectrum and the spatio-temporal spectrum is found to be:

$$W(f) = \iint \mathrm{d}\vec{\kappa}\, u(\vec{\kappa}, f). \tag{A.10}$$

Substituting Eq (A.6) into Eq (A.10) and switching to a polar integral representation:

$$W(f) = \int_0^\infty \mathrm{d}\kappa\, \kappa \int_{-\pi}^{\pi} \mathrm{d}\theta\, \delta\left(f + \frac{\vec{\kappa} \cdot \vec{v}}{2\pi}\right) F(\vec{\kappa}). \tag{A.11}$$

Assuming $u(\vec{\kappa}, f) = u(\kappa, f)$, and utilizing the evenness of the θ integration, the temporal frequency spectrum can be rewritten as:

$$W(f) = \int_0^\infty \mathrm{d}\kappa\, \kappa F(\kappa)\, 2\int_0^\pi \mathrm{d}\theta\, \delta\left(f + \frac{\kappa v}{2\pi}\cos\theta\right). \tag{A.12}$$

Making a change in variables,

$$W(f) = 2\int_0^\infty \mathrm{d}\kappa\, \kappa F(\kappa) \int_{-1}^{1} \frac{\mathrm{d}\lambda}{(1-\lambda^2)^{1/2}} \frac{2\pi}{\kappa v}\, \delta\left(\lambda + \frac{2\pi f}{\kappa v}\right) \tag{A.13}$$

where $\lambda = \cos\theta$ and the relation $\delta\left(f + \frac{\kappa v \lambda}{2\pi}\right) = \frac{2\pi}{\kappa v}\delta\left(\lambda + \frac{2\pi f}{\kappa v}\right)$ has been used. This simplifies to

$$W(f) = \frac{4\pi}{v}\int_{\frac{2\pi|f|}{v}}^\infty \frac{\mathrm{d}\kappa\, \kappa F(\kappa)}{\left(\kappa^2 - \left(\frac{2\pi f}{v}\right)^2\right)^{1/2}}. \tag{A.14}$$

Making the variable substitution $\kappa = \sqrt{k_t^2 + \left(\frac{2\pi f}{v}\right)^2}$ we write the equivalent form

$$W(f) = \frac{8\pi}{v}\int_0^\infty \mathrm{d}\kappa_t\; F\left(\sqrt{\kappa_t^2 + \left(\frac{2\pi f}{v}\right)^2}\right). \tag{A.15}$$

Eqs (A.14) and (A.15) will be used as the means to find the temporal equivalent spectrum of a filtered isotropic two dimensional spatial spectrum in Chapter III.

For the three dimensional spatial spectrum, Tartarski finds an expression equivalent to that derived in Eqs (A.14) and (A.15) for a two dimensional spatial spectrum.

$$W(f) = \frac{4\pi^2}{v}\int_{\frac{2\pi|f|}{v}}^\infty \mathrm{d}\kappa\, \kappa\, \Phi(\kappa) \tag{A.16}$$

where $\Phi(\kappa)$ represents an isotropic three dimensional spatial spectrum. Using the relation (17)

$$\frac{\mathrm{d}}{\mathrm{d}\omega}\int_{\phi_1(\omega)}^{\phi_2(\omega)} \mathrm{d}\kappa\, F(\kappa,\omega) = \int_{\phi_1(\omega)}^{\phi_2(\omega)} \mathrm{d}\kappa\, \frac{\partial F}{\partial \omega} + F(\phi_2,\omega)\frac{\mathrm{d}\phi_2}{\mathrm{d}\omega} - F(\phi_1,\omega)\frac{\mathrm{d}\phi_1}{\mathrm{d}\omega} \tag{A.17}$$

Tatarski finds the inverse relation to be

$$\Phi(\kappa) = -\frac{v^2}{8\pi^3\kappa} W'\left(\frac{\kappa v}{2\pi}\right). \tag{A.18}$$

Unfortunately, Eq (A.17) can not be similiarly applied to Eq (A.14) to find the temporal spectrum equivalent of the isotropic two dimensional spatial spectrum. This is because of the more complex integral argument of Eq (A.14) involving the temporal frequency variable f. Knowing the three dimensional spatial spectrum equivalent of the temporal spectrum from Eq (A.18), a relationship between $\Phi(\kappa)$ and $F(\kappa)$ is developed instead. Given the Fourier transform relation:

$$\Gamma(\vec{r}) = \iiint \mathrm{d}\vec{\kappa}\, \cos(\vec{\kappa}\cdot\vec{r})\, \Phi(\vec{\kappa}) \tag{A.19}$$

where $\Gamma(\vec{r})$ is a three dimensional spatial correlation and $\vec{r} = (\Delta x, \Delta y, \Delta z)$, the two dimensional correlation can be found from:

$$\Gamma(\Delta x, \Delta y, 0) = B(\Delta x, \Delta y) = \iint \mathrm{d}\kappa_x\, \mathrm{d}\kappa_y\, \cos(\kappa_x \Delta x + \kappa_y \Delta y) \left[\int \mathrm{d}\kappa_z\, \Phi(\vec{\kappa})\right]. \tag{A.20}$$

The relationship between the two dimensional and three dimensional spatial spectrum is found to be:

$$F(\kappa_x, \kappa_y; z) = \int \mathrm{d}\kappa_z\, \Phi(\kappa_x, \kappa_y, \kappa_z). \tag{A.21}$$

Finally, we determine the inverse relation of Eq (A.15) by substituting Eq (A.18) in Eq (A.21):

$$F(\kappa_t) = -\int \mathrm{d}\kappa_z\, \frac{v^2}{8\pi^3\kappa} W'\left(\frac{v\sqrt{\kappa_t^2 + \kappa_z^2}}{2\pi}\right) \tag{A.22}$$

where $\Phi(\kappa) = \Phi\left(\sqrt{\kappa_t^2 + \kappa_z^2}\right)$ and $\kappa_t^2 = \kappa_x^2 + \kappa_y^2$.

In summary, this section has developed the mathematical means to convert a temporal spectrum to an equivalent isotropic two dimensional spatial spectrum through the application of Eqs (A.18) and (A.21) and then

revert back to an equivalent temporal spectrum by Eq (A.14). The necessary assumption for these transformations was only that of frozen field flow.

Bibliography

1. Coulman, C. E. and others. "Outer Scale of Turbulence Appropriate to Modeling Refractive-Index Structure Profiles," *Appl. Opt.*, *27*:155-160 (1988).
2. Fried, D. L. "Time-delay-induced mean-square error in adaptive optics," *J. Opt. Soc. Am A*, *7*:1224-1225 (1990).
3. Fried, D. L. and G. E. Mevers. "Evaluation of r_o for Propagation Down Through the Atmosphere," *Appl. Opt.*, *13*:2620-2622 (1965).
4. Gardner, C. S., et al. "Design and Performance Analysis of Adaptive Optical Telescopes Using Laser Guide Stars," *Proc. IEEE*, *78*:1721-1743 (1990).
5. Goodman, J. W. *Statistical Optics*. New York: John Wiley & Sons, 1985.
6. Greenwood, D. P. "Bandwidth Specification for Adaptive Optics Systems," *J. Opt. Soc. Am.*, *67*:390-393 (1977).
7. Greenwood, D. P. "Measurements of Atmospheric Phase and Tilt, and Comparison with Theory," *ESO Conference and Workshop Proceedings*, *30*:675-682 (1988).
8. Greenwood, D. P. and D. L. Fried. "Power spectra requirements for wave-front-compensation systems," *J. Opt. Soc. Am.*, *66*:193-206 (1976).
9. Hardy, J. H. "Active Optics: A New Technology for the Control of Light," *Proc. IEEE*, *66*:651-697 (1978).
10. Hudgin, R. H. "Wave front compensation error due to finite corrector-element size," *J. Opt. Soc. Am.*, *67*:393-395 (1977).
11. Karr, T. J. "Temporal response of atmospheric turbulence compensation," *Appl. Opt.*, *30*:363-364 (1991).
12. Lee, R. W. and J. C. Harp. "Weak scattering in random media, with applications to remote probing," *Proc. IEEE*, *57*:375-406 (1969).
13. Moore, Kenneth E. and George N. Lawrence. "Zonal Model of an Adaptive Optical Mirror," *Appl. Opt.*, *29*:4622-4628 (1990).
14. Noll, Robert J. "Zernike Polynomials and Atmospheric Turbulence," *J. Opt. Soc. Am.*, *66*:207-211 (1976).
15. Roddier, F. "The Effects of Atmospheric Turbulence in Optical Astronomy," *Progress in Optics XIX*, edited by E. Wolf, New York: North-Holland, 1981.
16. Roggemann, M. C. "Limited degree-of-freedom adaptive optics and image reconstruction," *Appl. Opt.*, *30*:4227-4233 (1991).
17. Spiegel, Murray R. *Mathematical Handbook of Formulas and Tables*. New York: McGraw-Hill, 1968.
18. Tatarski, V. I. *The Effects of the Turbulent Atmosphere on Wave Propagation*. Jerusalem: Israel Program for Scientific Translations, 1971.
19. Tyson, R. K. "Adaptive optics system performance approximations for atmospheric turbulence correction," *Opt. Eng.*, *29*:1165-1173 (1990).
20. Welsh, B. M. "The Effect of an Adaptive Optical System's Temporal Response on Imaging Performance," *SPIE proceedings1688*. 1992.
21. Welsh, B. M. and C. S. Gardner. "Performance Analysis of Adaptive Optics Systems using Slope Sensors," *J. Opt. Soc. Am. A*, *6*:1913-1923 (1989).
22. Welsh, B. M. and C. S. Gardner. "Effects of turbulence induced anisoplanatism on the imaging performance of adaptive astronomical telescopes using laser guide stars," *J. Opt. Soc. Am. A*, *8*:69-80 (1991).

Vita

Patrick Harrington received a B.S.E. degree from the University of Michigan in electrical engineering, April 1988. Upon graduation, he was commissioned as a lieutenant in the United States Air Force. He was promoted to the rank of captain in 1992. He entered the School of Engineering at the Air Force Institute of Technology, Wright-Patterson Air Force Base, Ohio, in May 1991.

Permanent address: none

REPORT DOCUMENTATION PAGE

Form Approved
OMB No. 0704-0188

1. AGENCY USE ONLY (Leave blank)	2. REPORT DATE	3. REPORT TYPE AND DATES COVERED
	December 1992	Master's Thesis

4. TITLE AND SUBTITLE
THE EFFECT OF AN ADAPTIVE OPTICAL SYSTEM'S SPATIO-TEMPORAL RESPONSE ON IMAGING PERFORMANCE

5. FUNDING NUMBERS

6. AUTHOR(S)
Patrick Michael Harrington, Captain, USAF

7. PERFORMING ORGANIZATION NAME(S) AND ADDRESS(ES)
Air Force Institute of Technology, WPAFB OH 45433-6583

8. PERFORMING ORGANIZATION REPORT NUMBER
AFIT/GEO/ENG/92D-06

9. SPONSORING/MONITORING AGENCY NAME(S) AND ADDRESS(ES)
Captain Mike Roggemann
PL/LIMI
Kirtland AFB, NM 87117

10. SPONSORING/MONITORING AGENCY REPORT NUMBER

11. SUPPLEMENTARY NOTES

12a. DISTRIBUTION/AVAILABILITY STATEMENT
Distribution Unlimited

12b. DISTRIBUTION CODE

13. ABSTRACT (Maximum 200 words)
Ideally, an adaptive optical control system would have instantaneous temporal response and infinite spatial bandwidth. In real systems, the response time of the adaptive optical control system is limited by the integration time of the wave front sensor, the computational time of the control algorithm, and the actuator response time. Additionally, finite inter actuator spacing limits the deformable mirror's ability to reproduce spatial frequencies having a period less than twice this spacing. Although analyses general enough to account for both the temporal and spatial characteristics of the adaptive optical system exist, they are complex and require detailed information regarding the wave front sensor, the deformable mirror, and the control algorithm. This investigation develops a frequency domain model that describes performance effects of an adaptive optical system's temporal response taking into account aperture piston and tilt removal and spatial bandwidth limitations due to finite subaperture size. The unique aspect of this model is the relative ease with which performance characteristics of different spatial and temporal system response functions can be investigated.

14. SUBJECT TERMS
Atmospheric Optics, Atmospheric Motion, Adaptive Optics, Phase Detectors, Correlation

15. NUMBER OF PAGES
49

16. PRICE CODE

17. SECURITY CLASSIFICATION OF REPORT	18. SECURITY CLASSIFICATION OF THIS PAGE	19. SECURITY CLASSIFICATION OF ABSTRACT	20. LIMITATION OF ABSTRACT
UNCLASSIFIED	UNCLASSIFIED	UNCLASSIFIED	UL